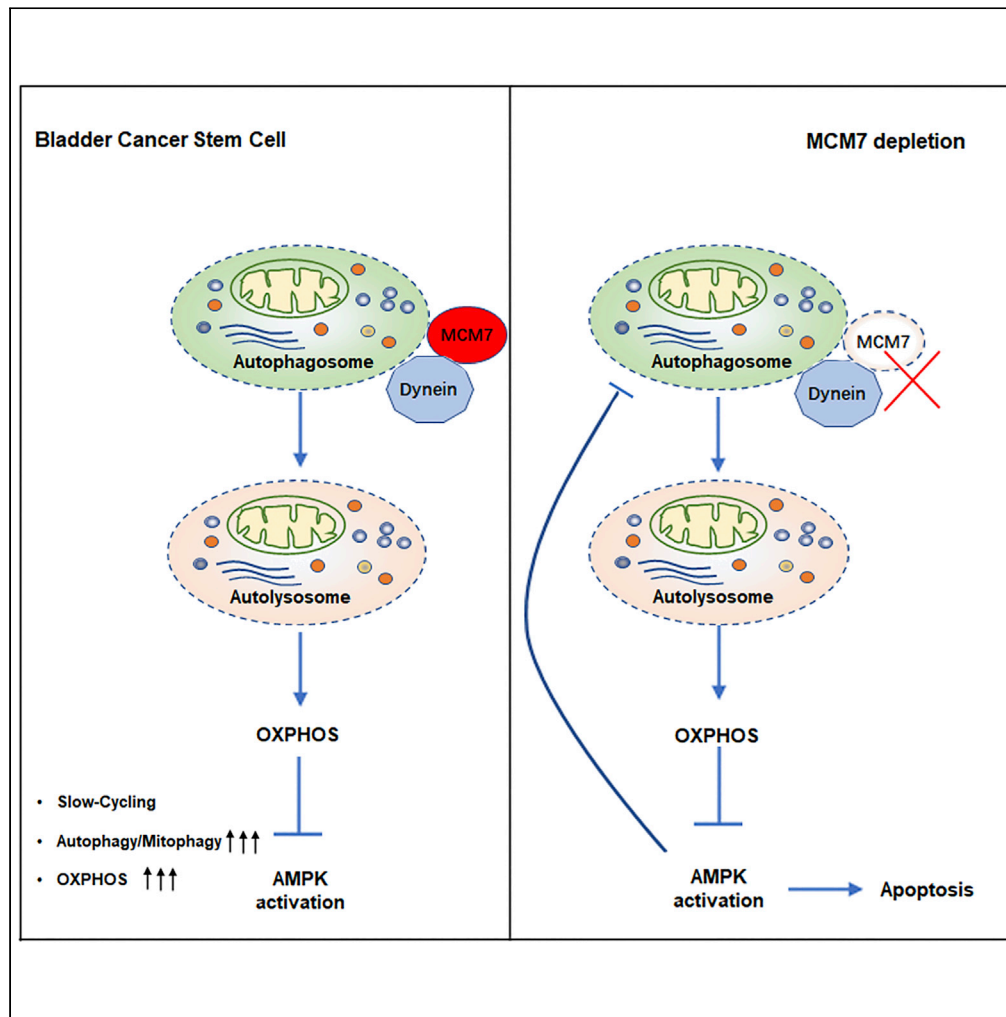


Article

MCM7 supports the stemness of bladder cancer stem-like cells by enhancing autophagic flux



Lijun Mo, Bijia Su, Lili Xu, Zhiming Hu, Hongwei Li, Hongyan Du, Jinlong Li

dhy48321@smu.edu.cn (H.D.)
lijinlong@smu.edu.cn (J.L.)

Highlights

Enhancement of autophagy and mitophagy in bladder cancer stem-like cells (BCSLCs)

The autophagy/mitophagy sustains BCSLCs stemness

MCM7 facilitates autophagic flux to support BCSLCs stemness



Article

MCM7 supports the stemness of bladder cancer stem-like cells by enhancing autophagic flux

Lijun Mo,^{1,2,3} Bijia Su,¹ Lili Xu,¹ Zhiming Hu,¹ Hongwei Li,¹ Hongyan Du,^{1,*} and Jinlong Li^{1,*}

SUMMARY

Autophagy plays critical roles in the pluripotent stemness of cancer stem cells (CSCs). However, how CSCs maintain the elevated autophagy to support stemness remains elusive. Here, we demonstrate that bladder cancer stem-like cells (BCSLCs) are at slow-cycling state with enhanced autophagy and mitophagy. In these slow-cycling BCSLCs, the DNA replication initiator MCM7 is required for autophagy and stemness. MCM7 knockdown inhibits autophagic flux and reduces the stemness of BCSLCs. MCM7 can facilitate autolysosome formation through binding with dynein to promote autophagic flux. The enhanced autophagy/mitophagy helps BCSLCs to maintain mitochondrial respiration, thus inhibiting AMPK activation. AMPK activation can trigger switch from autophagy to apoptosis, through increasing BCL2/BECLIN1 interaction and inducing P53 accumulation. In summary, we find that MCM7 can promote autophagic flux to support.

INTRODUCTION

Bladder cancer (BC) is one of the most common life-threatening malignancies in men. According to Tumor Statistics (2021), there were 83,730 new cases and 17,200 deaths of this disease in the United States (Siegel et al., 2021). Combination strategy including surgery, chemotherapy, and immunotherapy is currently the therapeutic option for BC patients (Parikh et al., 2019). Unfortunately, a majority of patients still experience disease relapse and ultimately die of tumor metastasis (James et al., 2012). The cancer stem cells (CSCs) which have strong self-renewal capability are the main source of tumor recurrence and metastasis and therefore stand as a main obstacle for cancer elimination (Zhang et al., 2019).

Autophagy, a fundamental catabolic process, plays key roles in the maintenance of intracellular homeostasis by degrading and recycling damaged cytoplasmic components (Kudo et al., 2020; Yamamoto et al., 2020). Substantial evidence implicates that autophagy is a protective mechanism of tumor cells against radiation and chemotherapy (Han et al., 2018; Najafi et al., 2019; Nazio et al., 2019). Autophagy is enhanced in various CSCs, including pancreatic cancer (Li et al., 2020), colorectal cancer (Olejniczak-Kęder et al., 2019; Qureshi-Baig et al., 2020), leukemia (Kim et al., 2020), and glioblastoma (Angeletti et al., 2016; Carballo and Ribeiro, 2020). Consistently, inhibition of autophagy can reduce the CSCs stemness (Liu et al., 2017; Nazio et al., 2019; Praharaj et al., 2021). Mechanistically, autophagy promotes stemness by preventing senescence (Garcia-Prat et al., 2016), reducing ROS (Whelan et al., 2017), enhancing metabolic plasticity (Alcala et al., 2020) and inhibiting p53 (Liu et al., 2017). Although the relationship between autophagy and CSCs has been established, the underlying mechanisms fail to reach consensus in different CSCs. Besides, it is unclear how CSCs maintain the elevated autophagy to support stemness.

Minichromosome maintenance proteins (MCMs), including MCM2-7, form hexamer complexes and act as helicase to unwind DNA during replication (Li and Xu, 2019). Although MCMs are well known as replicative helicase, their overabundance and distribution patterns on chromatin present a paradox, the "MCM paradox" (Das et al., 2014), indicative of additional MCMs functions. Indeed, other functions of MCMs have been revealed recently. Among them, the contributions of MCM7 to malignant transformation are attractive. MCM7 participates in DNA damage repair (Guan et al., 2017; Liang et al., 2017; Parlanti et al., 2007), promotes metastasis of cancer cells (Wang et al., 2019), and is positively correlated with malignant progression (Qu et al., 2017; Ren et al., 2006). Inhibition of MCM7 reduces the stemness of liver CSCs (Wang et al., 2019). Recently, MCM7 has been reported to regulate autophagy in fibroblasts (Dumit et al., 2014). Given the supportive effect of autophagy on stemness, we reason that MCM7 may regulate autophagy so as to support CSCs stemness.

¹Institute of Biotherapy, School of Laboratory Medicine and Biotechnology, Southern Medical University, 1023 Sha Tai Road, Guangzhou, Guangdong 510515, China

²Department of Clinical Laboratory, Dermatology Hospital, Southern Medical University, Guangzhou, Guangdong, China

³Lead contact

*Correspondence: dhy48321@smu.edu.cn (H.D.), lijnlong@smu.edu.cn (J.L.)
<https://doi.org/10.1016/j.isci.2022.105029>



Here, we investigated the contributions of MCM7 and autophagy on stemness in bladder cancer stem-like cells (BCSLCs). Our results showed that autophagy assisted BCSLCs to maintain stemness by promoting mitochondrial homeostasis and thereby inhibiting AMPK mediated P53 accumulation. MCM7 contributes to BCSLC stemness by promoting autophagic flux, which presents as a way for BCSLC to maintain autophagy.

RESULTS

Bladder cancer stem-like cells (BCSLCs) are at slow-cycling status

Drug-resistant UMUC3 and EJ human bladder cancer cells were obtained by long-term cisplatin incubation. The resistant cells expressed high levels of drug-resistant genes including *ABCC1*, *ABCB1*, *TOP2B*, and *GSTK1* (Figure S1A), and resisted to the cytotoxicity of cisplatin as well as paclitaxel (Figure S1B). When these resistant cells were exposed to higher concentrations of cisplatin, the mRNA of the pluripotent genes including *NANOG*, *ABCG2*, *OCT4*, *CD133*, and *CD44* were up-regulated (Figure S1C), and $CD44^+$ or $CD133^+$ cell populations were increased (Figure S1D). Moreover, these resistant cells showed strong spheroid formation ability under non-adhesive culture *in vitro* (Figure S1E) and enhanced tumorigenesis in mice (Figure S1F). These data indicated that BCSLCs were enriched from the drug-resistant BC cells.

Both BCSLCs, including EJ-CSLC and UMUC3-CSLC, were at slow-cycling status shown by G_0/G_1 phase arrest (Figure 1A), reduced EdU incorporation (Figure 1B), and decreased protein levels of Cyclin B and Cyclin D (Figure 1C). Accordingly, in these slow-cycling BCSLCs, members of the MCMs (MCM2 and MCM3) were dramatically down-regulated whereas MCM7 levels was not reduced, suggesting that MCM7 may be associated with the BCSLCs stemness (Figures 1C and S2A).

MCM7 involves in stemness of BCSLCs

Next, we explored whether MCM7 was involved in the stemness of BCSLCs. MCM7 knockdown by siRNA significantly reduced the mRNA levels of stemness-related genes (*NANOG*, *ABCG2*, *OCT4*, *CD133*, and *CD44*) (Figures 2A and S2B), decreased both $CD133^+$ and $CD44^+$ cell populations (Figure 2B), and down-regulated the protein levels of *OCT4*, *SOX2*, and *NANOG* (Figure 2C). In addition, MCM7 knockdown induced apoptosis (Figure 2D) and markedly reduced the spheroid formation ability of BCSLCs (Figure 2E). These findings indicate that MCM7 is involved in stemness of BCSLCs.

Autophagy is activated in BCSLCs and contributes to stemness

Accumulating studies reported that autophagy plays important roles in stemness of tumor cells (Han et al., 2018; Najafi et al., 2019; Nazio et al., 2019). We thus analyzed the autophagy-related genes (ARGs) expression in TCGA bladder cancers. It showed that 38 ARGs were differentially expressed in the bladder cancer tissues compared with normal controls (Figures 3A and 3B). Moreover, patients with differential expression of the ARGs (high risk) had poor prognosis (Figure 3C).

Subsequently, we detected autophagy in the BCSLCs. The expression of autophagy-regulating genes *BECLIN1* and *ATG7* were up-regulated in BCSLCs (Figure 3D). Western blot analysis showed increased conversion of LC3-I to LC3-II and decreased P62 level (Figure 3E). Consistently, immunofluorescence showed enhanced LC3 puncta (Figure 3F) and decreased P62 accumulation (Figure 3G) in BCSLCs. Moreover, the LC3 puncta was inhibited by 3-MA but further accumulated by chloroquine, indicating that the enhanced LC3 puncta was not because of blockage of autophagic flux (Figures 4A and 4B). The autophagic flux of BCSLCs was further investigated by mCherry-EGFP-LC3 tandem fluorescent indicator to monitor autolysosome maturation. The green fluorescence of the fusion protein is quickly quenched in the acidic environment of autolysosomes, so just red fluorescence could be detected in the autolysosomes (Kimura et al., 2007). There was clearly elevated formation of autolysosomes (red fluorescence) in the BCSLCs, indicating an enhanced autophagic flux (Figure 4C). Next, the contribution of autophagy on BCSLCs stemness was studied. Autophagy inhibition by chloroquine significantly decreased the mRNA of stemness genes including *NANOG*, *ABCG2*, *OCT4*, *CD133*, and *CD44* (Figure 4D). Moreover, autophagy inhibition dramatically reduced the spheroid formation (Figure 4E). Together, these results indicate that enhanced autophagy promotes stemness of BCSLCs.

MCM7 interacts with dynein and facilitates autophagy flux in BCSLCs

It has been reported that MCM7 was involved in the regulation of autophagy in fibroblasts (Dumit et al., 2014). Thus, we reasoned that the unreduced MCM7 in the slow-cycling BCSLCs may regulate autophagy,

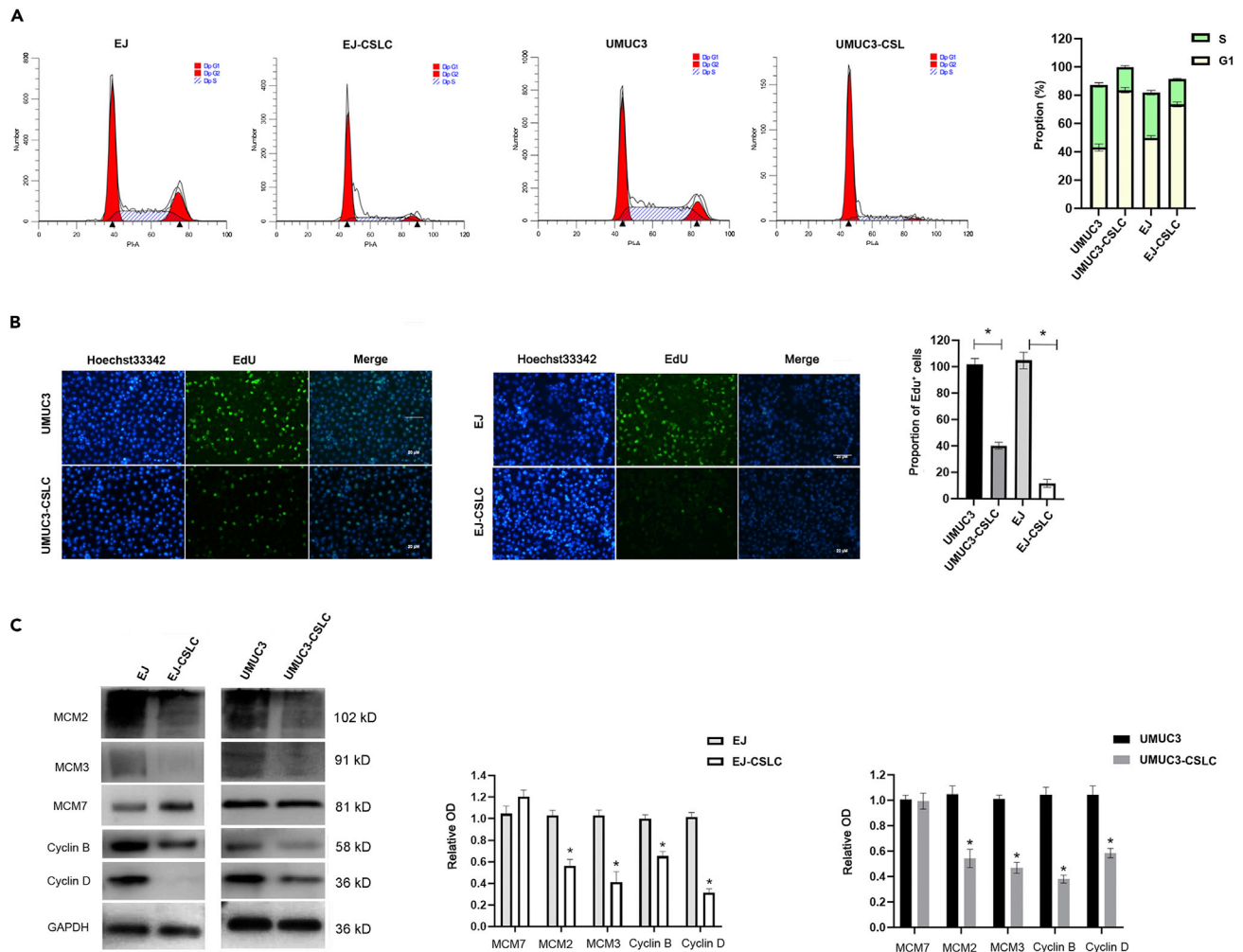


Figure 1. BCSLCs are at slow-cycling state

(A) Cell cycle of UMUC3, UMUC3 CSLC, EJ and EJ CSLCs were detected by flow cytometry.

(B) EdU was used to detect DNA replication.

(C) The expression of MCM2, MCM3, MCM7, Cyclin-B and Cyclin-D protein in BCSLCs was detected by western blot. Data are represented as mean \pm SEM, *p < 0.05.

helping to support stemness. As expected, MCM7 knockdown by siRNA significantly decreased the LC3 puncta (Figure 5A), reduced LC3-I to LC3-II conversion and increased P62 accumulation (Figure 5B). Moreover, the autolysosome maturation was blocked by MCM7 siRNA, which indicates that MCM7 could promote the autophagic flux by facilitating autolysosome maturation (Figure 5B).

Dynein is the major motor protein to mediate the autolysosome maturation by driving the retrograde transport of autophagosome along microtubules (Kimura et al., 2008; Mackeh et al., 2013). Thus, we tested whether MCM7 collaborates with dynein to promote autolysosome maturation. Co-IP assay revealed the interaction between MCM7 and dynein (Figure 5D). Moreover, dynein overexpression partially rescued the autolysosome maturation defect induced by MCM7 siRNA (Figure 5C). These results demonstrate that MCM7 can promote autophagic flux by binding with dynein to promote the autolysosome maturation.

Mitophagy and OXPPOS are enhanced in BCSLCs

The selective mitochondrial autophagy, namely mitophagy, can enhance metabolic plasticity so as to maintain the cell energy homeostasis (Alcala et al., 2020). Given that BCSLCs were at slow-cycling state, we

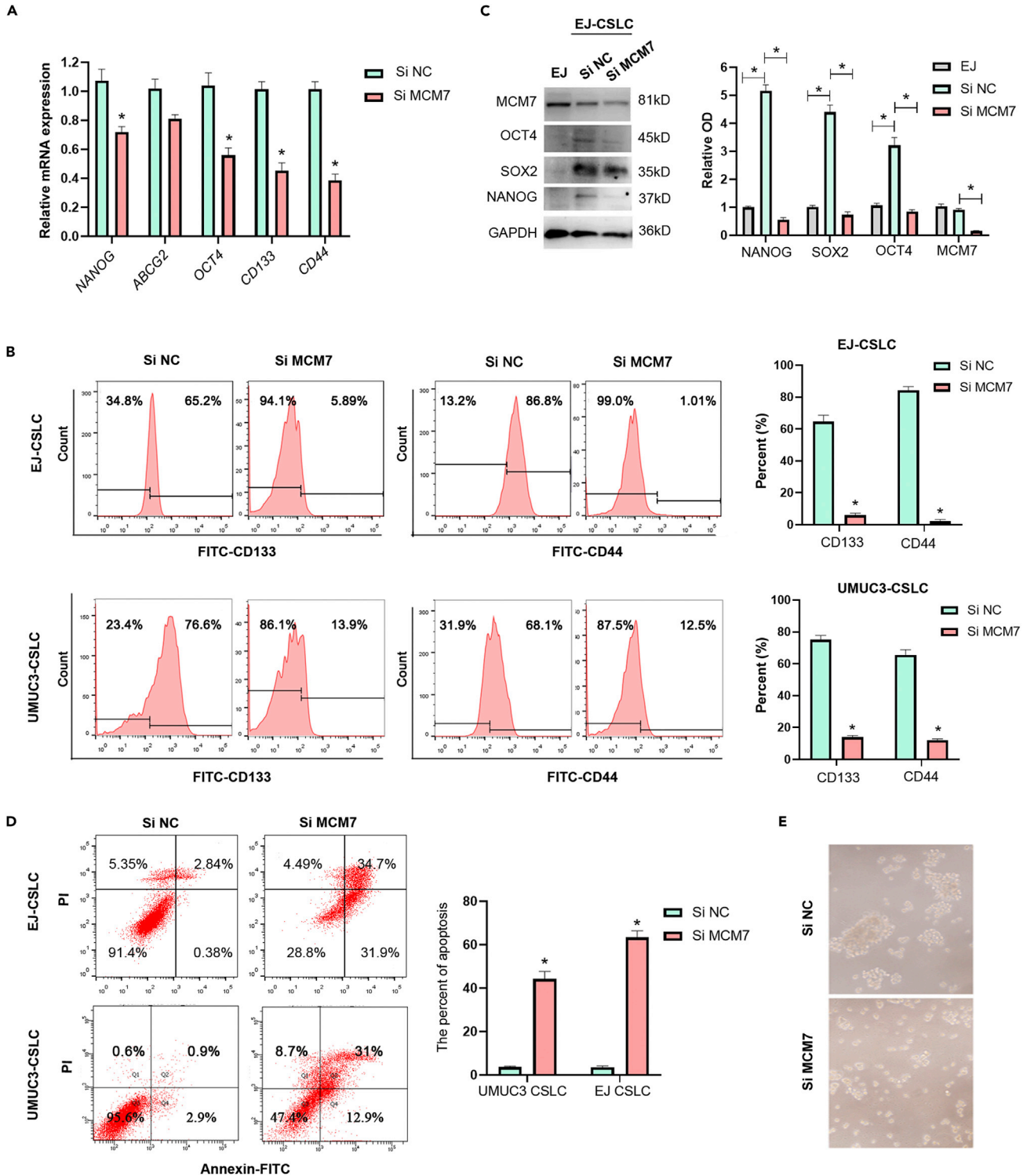


Figure 2. MCM7 is involved in stemness maintenance of BCSLCs

Cells were transfected with MCM7 siRNA for 24 h, (A) Real-time PCR was used to detect the expressions of stemness genes, *NANOG*, *ABCG2*, *OCT4*, *CD133* and *CD44*, with *GAPDH* as internal reference.

(B) Flow cytometry was used to detect the expression of *CD133* and *CD44*.

(C) Western blot was used to detect the protein levels of *NANOG*, *SOX2* and *OCT4* in EJ CSLC.

(D) Apoptosis was detected by flow cytometry.

(E) Tumor sphere-formation ability was tested in EJ CSLC. Data are represented as mean \pm SEM, * $p < 0.05$.

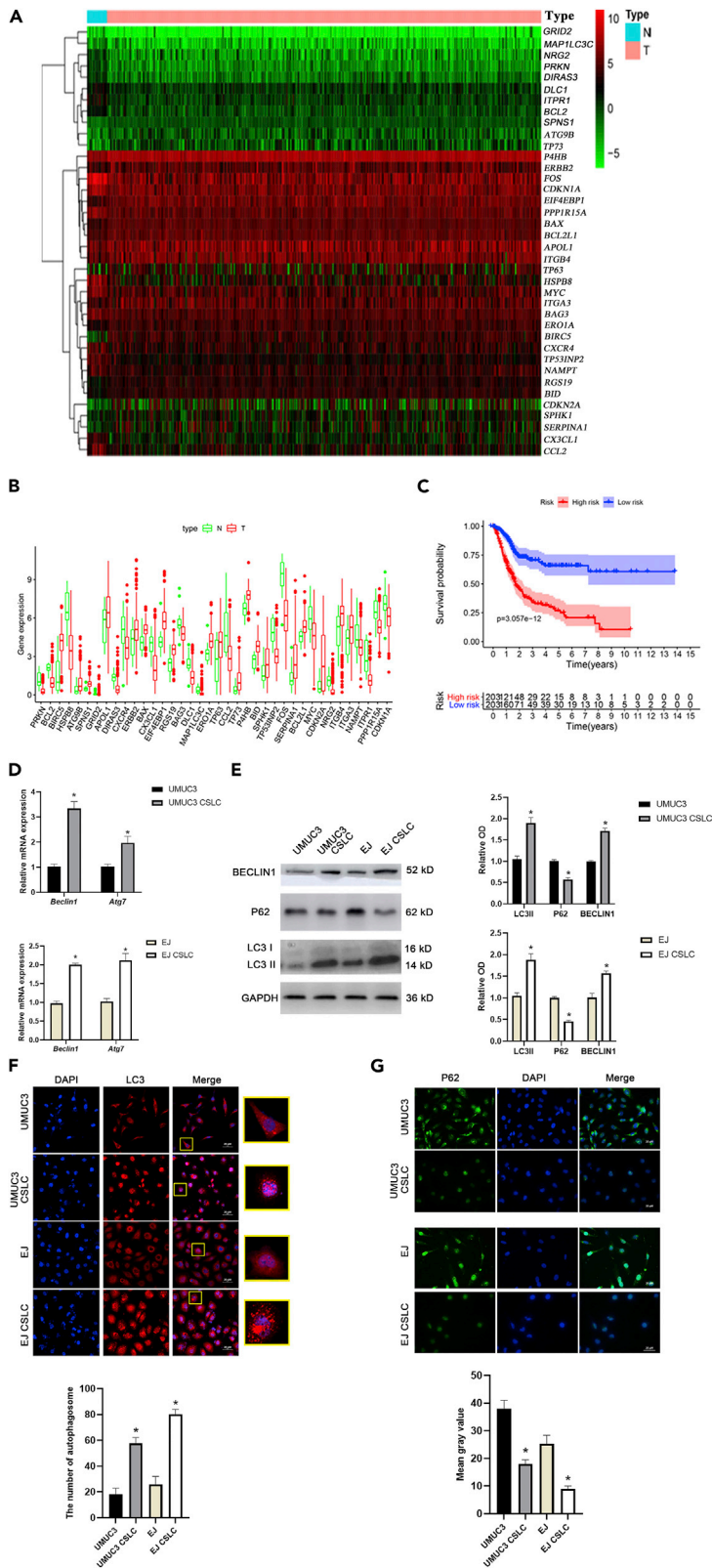


Figure 3. The autophagy of BCSLCs is enhanced

(A) Heatmap and (B) boxplot of differentially expressed ARGs in bladder cancer and paired no-tumor tissue. Differentially expressed genes were screened with thresholds of $|\log_2$ fold change (FC)| > 1 and adjusted p value < 0.05. (C) Kaplan–Meier plot represents those patients in the high-risk group had significantly shorter overall survival than those in the low-risk group. (D) The mRNA of *BECLIN1* and *ATG7* in BCSLCs was detected by q-PCR. (E) Protein levels of *BECLIN1*, *LC3* and *P62* were detected by western blot. (F) Immunofluorescence detection of autophagosomes in BCSLCs, red: *LC3*, blue: *DAPI*. (G) Immunofluorescence detection of *P62* in BCSLCs, green: *P62*, blue: *DAPI*. Data are represented as mean \pm SEM, *p < 0.05.

further explored the mitophagy and the metabolic status of BCSLCs. *ATP5A* (a mitochondrial marker) staining was used to visualize the mitochondria. More small-sphere mitochondria were observed in the BCSLCs compared with the tubule-shape mitochondria in the parent cells, indicating a thread-grain transition of mitochondrial reticulum in BCSLCs (Figure 6A). Moreover, co-localization of mitochondria with autophagosome was evidenced in BCSLCs (Figure 6B). *BNIP3* mRNA, the mitophagy-related factor, was increased in the BCSLCs (Figure 6C). Also, protein levels of *BNIP3* and *PINK1* were significantly increased (Figure 6D). These data suggest that mitophagy is activated in BCSLCs.

Then, we analyzed the two main metabolic pathways in BCSLCs, i.e., oxidative phosphorylation (OXPHOS) and glycolysis. The expression of OXPHOS-related genes (*COX5B*, *PGC1A* and *CYTC1*) were significantly increased, whereas glycolysis-related genes (*PKM2* and *LDHA*) showed no significant difference in BCSLCs compared to parent cells (Figure 6E). The metabolic profiles of BCSLCs were tested using the Seahorse Mito Stress Test and Glycolysis Stress Test Kits. It showed that basal respiration (oxygen consumption rate, OCR) and ATP production of BCSLCs was much higher than those of parent cells (Figure 6F) whereas the basal glycolysis was lower in BCSLCs (Figure 6G). Together, our results showed that BCSLCs have enhanced OXPHOS capability and were characterized by a more aerobic phenotype. Next, we tested whether *MCM7* knockdown affects the OXPHOS of BCSLCs. *MCM7* knockdown by siRNA decreased the basal respiration only in EJ-CSLC, but not in UMUC3-CSLC. The ATP production showed no difference after *MCM7* knockdown in both BCSLCs (Figure S3).

Activation of AMPK switches autophagy to apoptosis

AMP-activated protein kinase (AMPK) is the intracellular energy sensor that is activated under energy stress. The enhanced OXPHOS in the BCSLCs may regulate AMPK activation. Next, we selected EJ-CSLC with more evidenced mitophagy to explore the AMPK profiles. As expected, AMPK was inactive in the BCSLCs, as confirmed by a decreased *p*-AMPK/AMPK ratio (Figure 7A). Moreover, inhibiting mitophagy with *mdvi-1* lead to AMPK activation, whereas promoting mitophagy with CCCP resulted in further AMPK inhibition (Figure 7B). Further, we activated the AMPK by metformin and observed obvious apoptosis of EJ-CSLC (Figure 7C). In the meantime, metformin also inhibited autophagy, indicating a switch of autophagy to apoptosis (Figure 7D).

BCL2 can exert anti-apoptosis or anti-autophagy effects through binding to different partners, namely *BAX* or *BECLIN1* (Maejima et al., 2013; Pattingre et al., 2005). AMPK has been reported to regulate the binding between *BCL2* and its partners (Zhang et al., 2016). Thus, AMPK may regulate the binding of *BCL2* with *BAX* or *BECLIN1*, thereby regulating the switch of autophagy to apoptosis in the BCSLCs. Our results showed that in line with the enhanced autophagy in the EJ-CSLC *BCL2*/*BECLIN1* interaction was reduced as compared to that in the parent cells. AMPK activation by metformin increased the *BCL2*/*BECLIN1* interaction in the EJ-CSLC (Figures 8A and 8B), which is consistent with its inhibitory effect on autophagy. However, the *BCL2*/*BAX* interaction showed no difference before and after AMPK activation (Figure 8A). Thus, the pro-apoptotic effect of AMPK activation was less likely through regulating *BCL2*/*BAX* interaction. We have previously reported that the circadian protein *CRY1* exerts anti-apoptotic effect in drug-resistant BC cells by promoting *P53* degradation (Jia et al., 2021). It is known that AMPK can phosphorylate and destabilize *CRY1* (Lamia et al., 2009; Takahashi, 2017). So, we wonder whether AMPK exert pro-apoptotic effect through regulating the *CRY1*-*P53* axis. As expected, AMPK activation (metformin or AICAR) significantly decreased the *CRY1* level and lead to *P53* accumulation. On the contrary, inhibition of AMPK (Compound C, CC) increased the *CRY1* and dramatically decreased the *P53* level (Figure 8C). Collectively, these results indicate that AMPK activation can inhibit autophagy

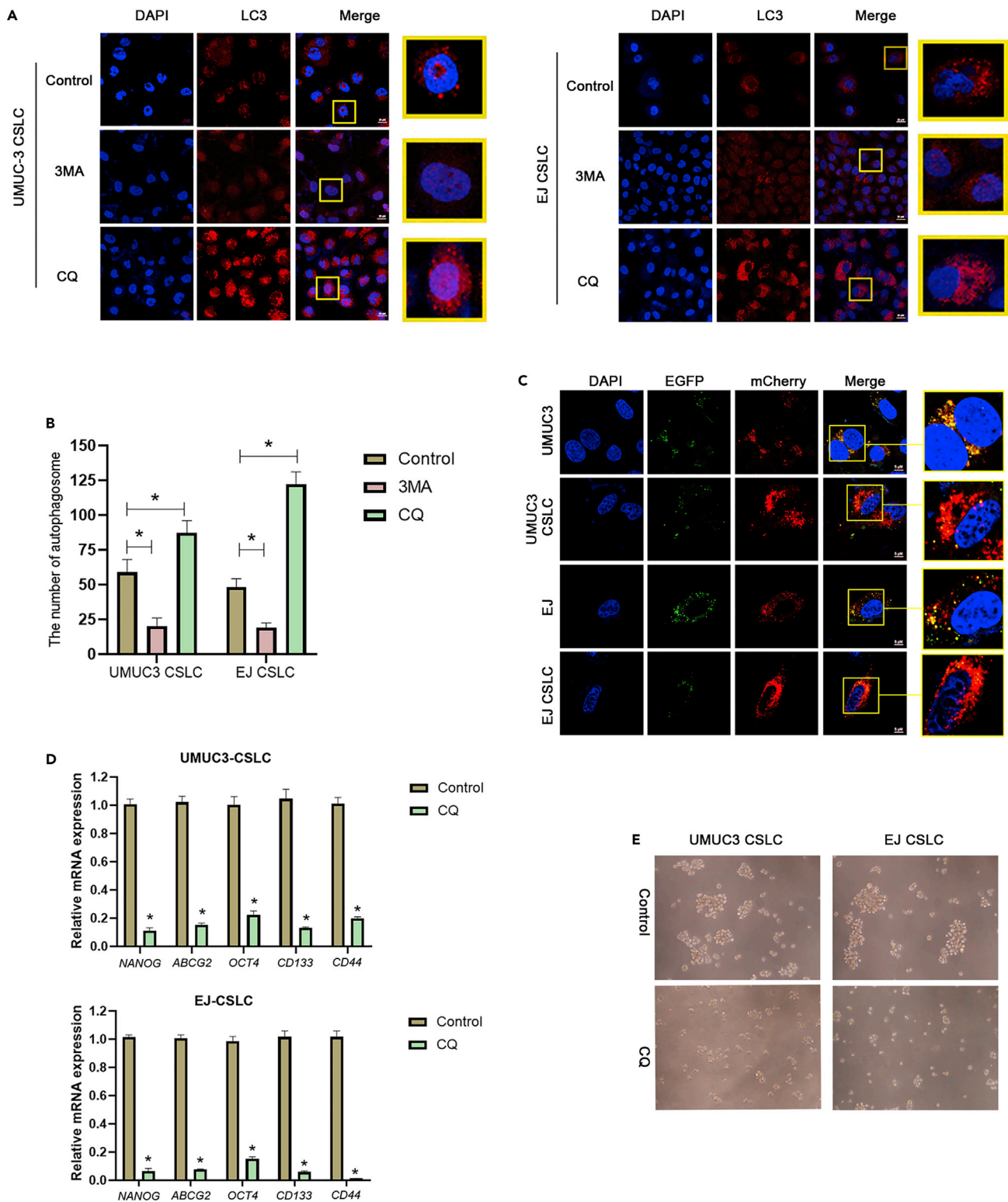


Figure 4. Autophagy inhibition reduces stemness of BCSLCs

(A) BCSLCs treated with 3MA or chloroquine for 24 h, immunofluorescence detection of autophagosomes; (B) The number of autophagosomes were presented by mean \pm SD.

(C) The autophagic flux of BCSLCs was detected using mCherry-EGFP-LC3 plasmid transfection. Red immunofluorescence represents autolysosome.

Figure 4. Continued

(D) BCSLCs were treated with chloroquine, the gene expression of pluripotent factors was detected by q-PCR, and tumor sphere-formation ability (E) was tested. Data are represented as mean \pm SEM, * $p < 0.05$.

by promoting BCL2/BECLIN1 interaction and induce apoptosis by promoting P53 accumulation, together leading to the switch from autophagy to apoptosis.

MCM7 silencing inhibits autophagy of BCSLCs *in vivo*

Finally, we detected the contribution of MCM7 on stemness in mice. Here, we used the recombinant lentivirus particles LV-MCM7 to silence MCM7. Three MCM7 shRNAs were prepared and LV-MCM7-1 was the most efficient one (Figures 9A and 9B). LV-MCM7-1 intratumoral injection significantly decreased the protein level of MCM7 as well as the stemness marker SOX2 (Figure 9C), and reduced the tumor volume in mice (Figures 9D and 9E). The regulatory effect of MCM7 on autophagy was also examined in the mice tumors. It showed that LC3 expression was significantly reduced (Figure 9F), whereas P62 protein was increased by LV-MCM7-1 (Figure 9G), indicating inhibition of autophagy in the tumors. Moreover, AMPK in the tumors were activated by LV-MCM7-1 (Figure 9H). These results demonstrated that silencing MCM7 could inhibit autophagy and reduce stemness *in vivo*.

DISCUSSION

Autophagy has emerged over the past several years as a requirement for stemness in CSCs. The mechanisms of autophagy supporting stemness and how CSCs maintain the elevated autophagy are still elusive (Smith and Macleod, 2019). Our study provides evidence that the BCSLCs have distinct proliferative and metabolic phenotype, characterized by slow-cycling, enhanced autophagy/mitophagy and OXPHOS capability. The enhanced autophagy/mitophagy and OXPHOS support stemness by inhibiting AMPK activation. Moreover, in the slow-cycling BCSLCs, we find a previously unrecognized function of MCM7 in promoting the autophagic flux, thus supporting the BCSLCs stemness.

Substantial evidences reveal that autophagy is critical for survival and stemness of CSCs (Smith and Macleod, 2019). More specifically, mitophagy, the selective mitochondrial autophagy, is the major adaptive mechanism of cancer cell to environmental stress by maintaining healthy mitochondrial functions (Chan, 2020). Notably, CSCs are more dependent on mitochondrial OXPHOS for energy production than non-CSCs (Sancho et al., 2016). In this study, the BCSLCs demonstrate enhanced autophagy and mitophagy. Also, the basal mitochondrial respiration and ATP production are enhanced, and the energy sensor AMPK does not be activated in BCSLCs. Moreover, inhibiting mitophagy can activate AMPK. Thus, it indicates that the enhanced mitophagy helps BCSLCs to maintain mitochondrial function therefore ensures cells have sufficient ATP for survival and inhibits AMPK from activation.

AMPK activation is well documented to induce autophagy. AMPK activation can promote cancer cell autophagy directly by phosphorylating autophagy-related proteins, or indirectly by regulating the expression of autophagy-related genes (Li and Chen, 2019). In these circumstances, the AMPK-induced autophagy is an adaptive mechanism of proliferating cancer cells in response to energetic stresses or mitochondrial insults, which is used to replenish ATP stores (Herzig and Shaw, 2018; Kim et al., 2011). However, in this research, because of the stressed culture condition (cisplatin), BCSLCs are in slow-cycling state and have enhanced OXPHOS. More importantly, the basal autophagy has been already activated in these BCSLCs. Therefore, AMPK activation should not further enhance autophagy, but alternatively, may trigger cell death program as a response to critical stress. Indeed, our results show that AMPK activation trigger switch from autophagy to apoptosis in the BCSLCs.

Our study provides evidence that the inhibitory effect of AMPK activation on autophagy in the BCSLCs is mediated by the BCL2/BECLIN1 binding. BCL2 can exert inhibitory effect on autophagy by binding with BECLIN1, whereas its binding with BAX inhibits apoptosis (Maejima et al., 2013; Pattingre et al., 2005). In this study, we demonstrate that AMPK activation increases the binding of BECLIN1 with BCL2. This is consistent with the inhibitory effect of AMPK activation on autophagy. However, the BCL2/BAX binding does not decrease, excluding the involvement of BCL2/BAX in the AMPK-induced apoptosis. Further, we demonstrate that AMPK activation significantly increases P53 protein level. Thus, the pro-apoptotic effect of AMPK activation may attribute to the increased P53 level.

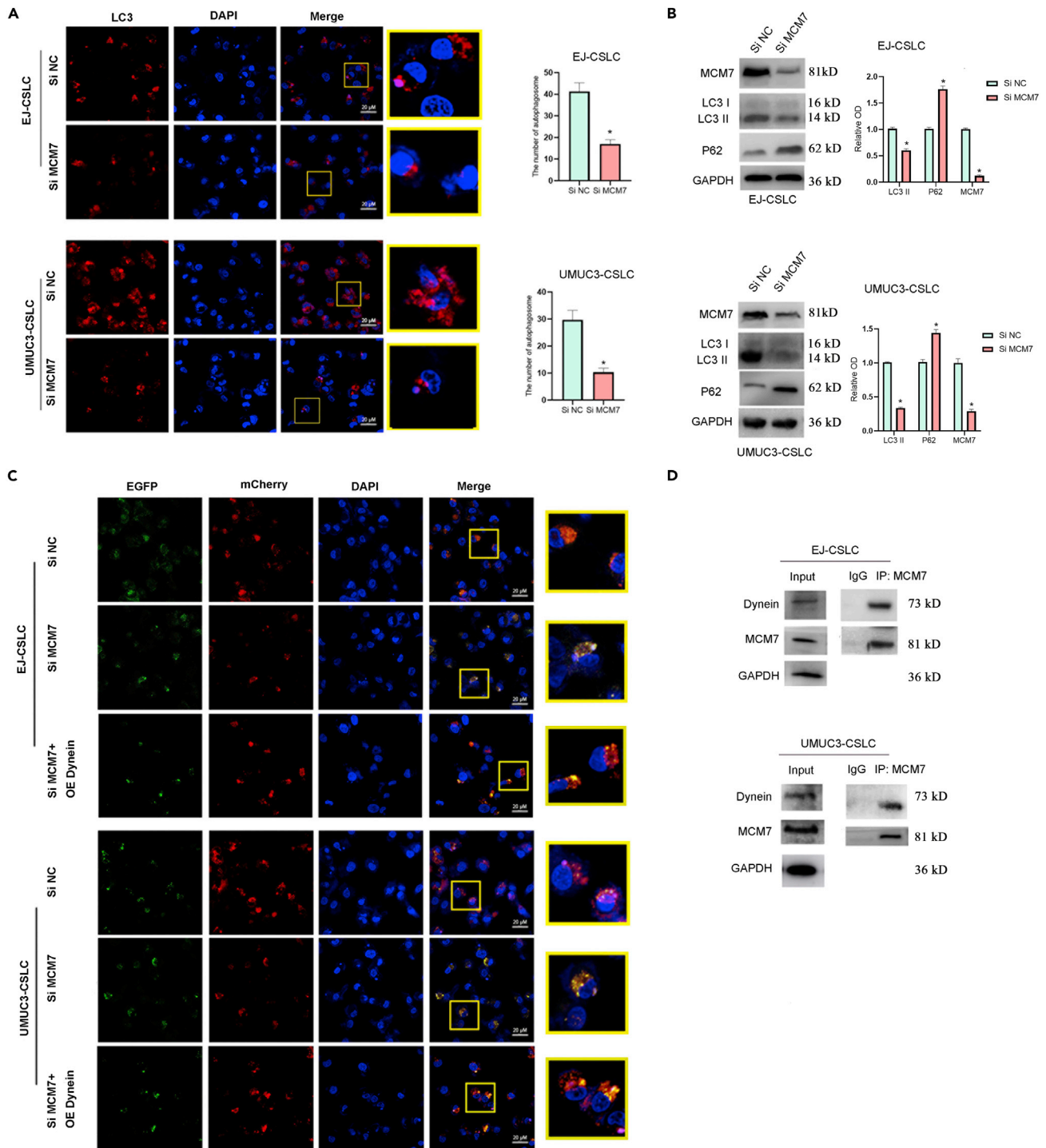


Figure 5. MCM7 silence inhibits autophagy of BCSLCs

(A) MCM7 was silenced by siRNA interfering for 24h in BCSLCs. The autophagosomes of BCSLCs were detected by Immunofluorescence and observed under confocal microscopy.
 (B) the expression of MCM7, LC3 and P62 were detected by western blot.
 (C) MCM7 was silenced by siRNA interfering together with or without dynein overexpression, the autophagic flux was detected by using mCherry-EGFP-LC3 plasmid transfection.
 (D) The total cell protein lysates of BCSLCs were co-immunoprecipitated with anti-MCM7 antibody, and then western blot was performed with dynein antibody to detect the interaction between the two proteins. Data are represented as mean \pm SEM, * $p < 0.05$.

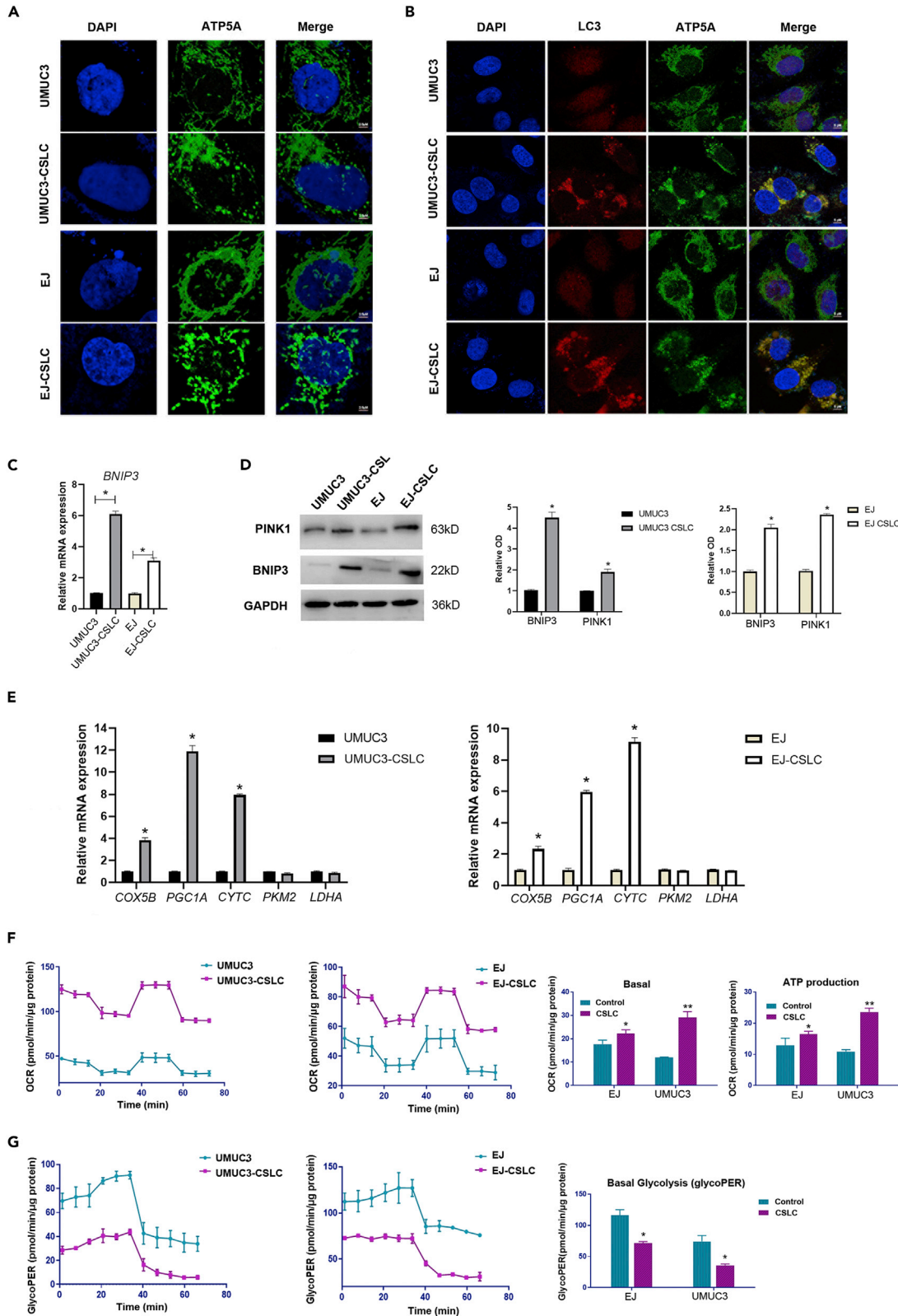


Figure 6. Mitophagy and OXPHOS are enhanced in BCSLCs

(A and B) Mitochondria was stained by ATP5A (green), autophagosomes were stained by LC3 (red), DNA was stained by DAPI (blue), and observed by confocal microscopy.
 (C) The expression of BNIP3 gene was detected by RT-PCR.
 (D) The expression of BNIP3 and PINK1 protein were detected by western blot.
 (E) The genes related to oxidative phosphorylation and glycolysis in BCSLCs were detected by RT-PCR.
 (F) The baseline, oligomycin-inhibited, FCCP-activated, and rotenone/antimycin A-inhibited OCR were analyzed by the Seahorse Mito Stress Test.
 (G) The baseline, rotenone/antimycin A-activated, and 2-deoxyglucose-inhibited ECAR values in these BCSLCs were captured by the Seahorse Glycolysis Stress Test. Data are represented as mean \pm SEM, * $p < 0.05$.

The MCMs form a hexameric structure composed of MCM2-7, which acts as helicase to initiate DNA replication (Li and Xu, 2019). In this study, the BCSLCs are in slow-cycling state with hampered DNA replication. Accordingly, members of the MCMs are dramatically down-regulated. However, MCM7 does not decrease. This suggest that the main function of MCM7 in these slow-cycling BCSLCs is not to initiate DNA replication, but instead, to participate in other functions associated with stemness. Our data reveal that MCM7 is required for stemness of BCSLCs. MCM7-knockdown can inhibit stemness of BCSLCs in both cell culture and mice model. Therefore, MCM7 participates in stemness maintenance. This can be further supported by a previous report that inhibition of MCM7 efficiently decreases liver CSCs traits (Wang et al., 2019).

The motor protein dynein play key role in the formation of autolysosome (Mackeh et al., 2013). Autophagosomes, including the mitophagosomes in mitophagy, are transported retrogradely along microtubules by microtubule-associated dynein to the perinuclear region (where lysosomes are dense), and finally fuse with lysosomes to form autolysosomes (Han et al., 2020; Kimura et al., 2008). In this study, MCM7-knockdown blocks the autophagic flux by impeding the formation of autolysosome. Further, we demonstrate that MCM7 interacts with dynein, and more importantly, dynein overexpression can rescue the autophagy defect caused by MCM7-knockdown. Therefore, MCM7 and dynein may work together on the microtubule to transport autolysosome, hence facilitating downstream autophagic flux. In line with this model, previous study shows that MCM7 co-localizes with microtubule (Zheng et al., 2017), and localizes to centrosomes (the major microtubule organizing center) in cancer cells (Kong et al., 2017). MCM7-promoted autophagy is also supported by another study reporting that lower level of MCM7 is correlated

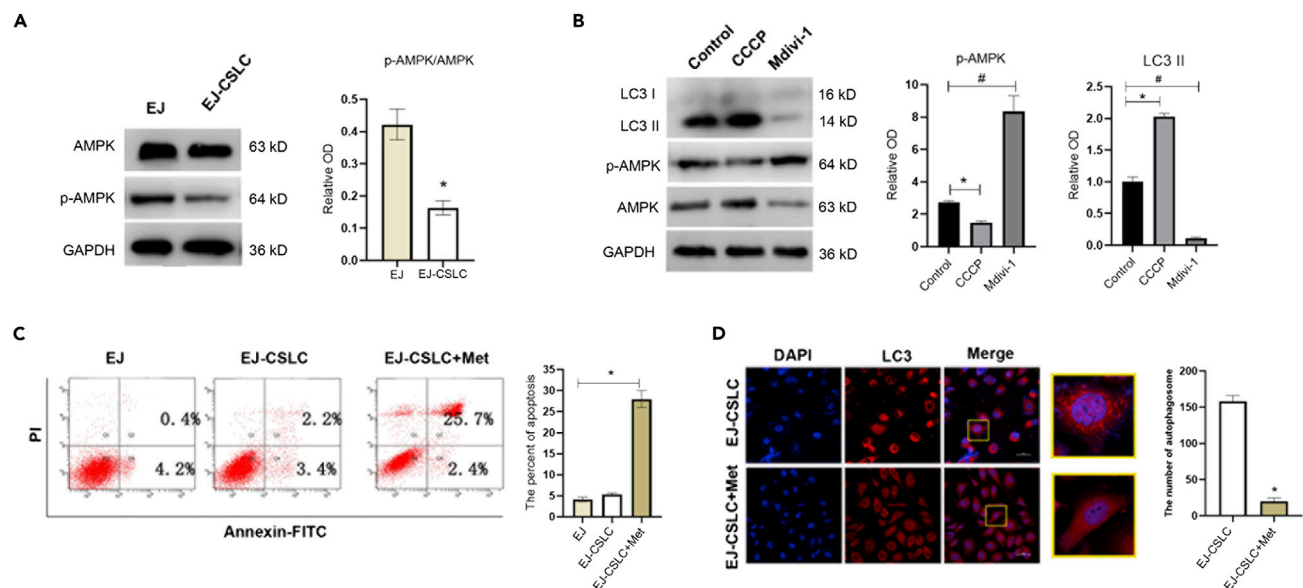
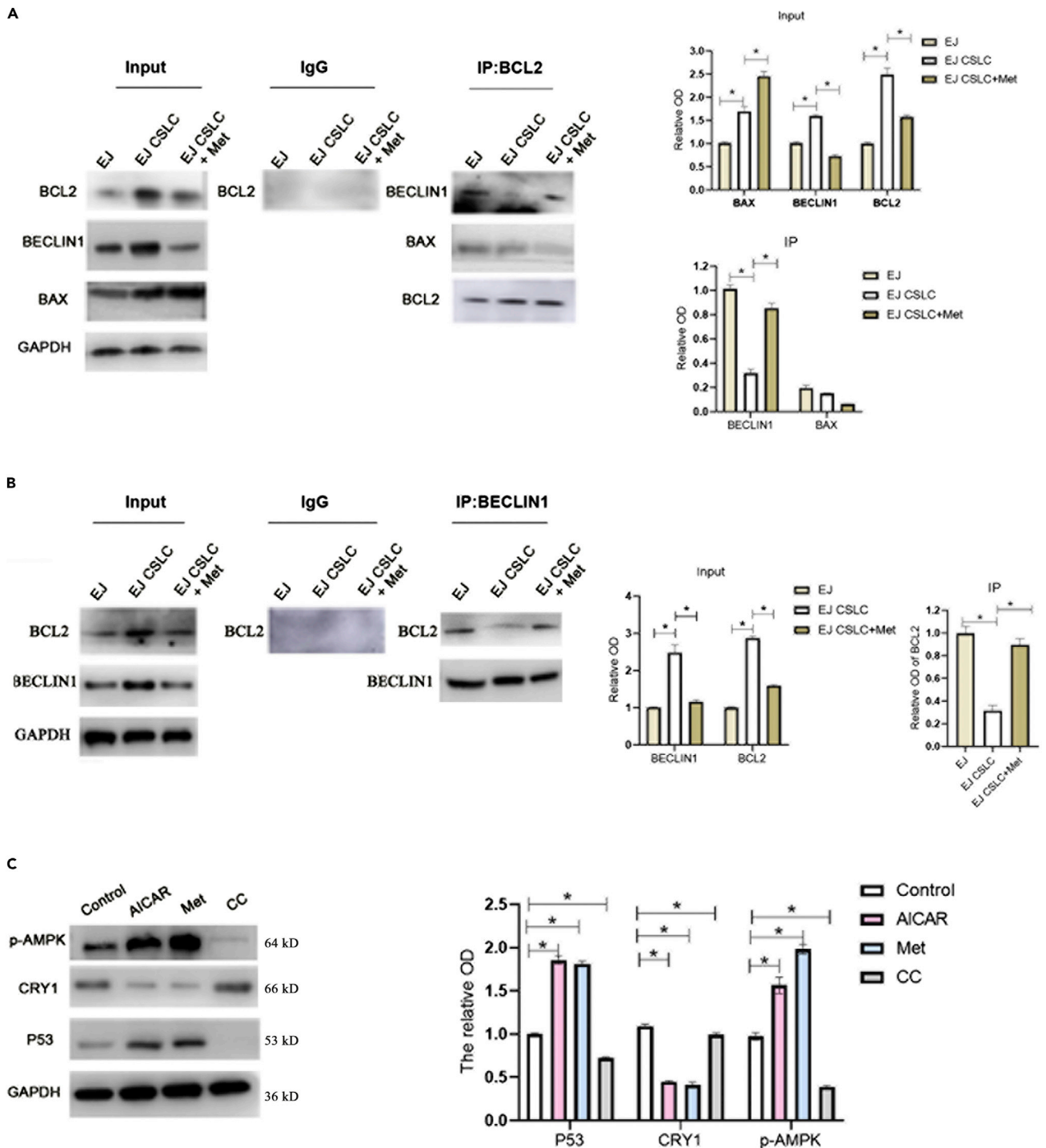


Figure 7. AMPK is not activated in BCSLCs

(A) Protein levels of AMPK and p-AMPK in EJ-CSLCs were detected by western blot.
 (B) EJ-CSLCs were treated with CCCP or Mdivi-1, and the protein levels of LC3, AMPK and p-AMPK were detected by western blot.
 (C) EJ-CSLC were treated with or without metformin for 24 h, cell apoptosis was detected by flow; and (D) the autophagosome was detected by Immunofluorescence, Met: Metformin. Data are represented as mean \pm SEM, * $p < 0.05$.



work in proliferating cancer cells? It is also unknown whether dynein shares overlapping or distinct binding domain of MCM7 with other MCMs. Moreover, as dynein exerts multifunction besides transporting autophagosome, such as regulating asymmetric/symmetric cell division, MCM7 may have other unknown functions by collaborating with dynein, meriting further exploration.

STAR★METHODS

Detailed methods are provided in the online version of this paper and include the following:

- KEY RESOURCES TABLE
- RESOURCE AVAILABILITY
 - Lead contact
 - Materials availability
 - Data and code availability
- EXPERIMENTAL MODEL AND SUBJECT DETAILS
- METHOD DETAILS
 - To obtain bladder cancer stem-like cells
 - Cell viability measurement
 - Spheroid formation
 - Quantitative real-time PCR
 - EdU incorporation assays
 - Immuno-fluorescence
 - Immunohistochemistry
 - Western blot
 - Flow cytometry analysis
 - Co-immunoprecipitation (Co-IP)
 - Analysis of autophagy related genes
 - Seahorse XF96 metabolic flux analysis
 - MCM7 silencing
 - Animal models
- QUANTIFICATION AND STATISTICAL ANALYSIS

SUPPLEMENTAL INFORMATION

Supplemental information can be found online at <https://doi.org/10.1016/j.isci.2022.105029>.

ACKNOWLEDGMENTS

This work was supported by the grants from the Natural Science Foundation of Guangdong Province (No. 2022A1515010515), National Natural Science Foundation of China (No. 81672915) and the grants from the Shenzhen science and technology project (JCYJ20180305164655077).

AUTHOR CONTRIBUTIONS

J.L., H.D., and H.L. designed experiments; L.M., B.S., L.X., and Z. H. carried out experiments; L.M., H.L., H.D., Z. H., B.S., and J.L. analyzed experiments results; J.L. and L.M. wrote the manuscript. All authors reviewed the manuscript.

DECLARATION OF INTERESTS

The authors declare no competing interests.

Received: March 29, 2022

Revised: July 7, 2022

Accepted: August 23, 2022

Published: September 16, 2022

REFERENCES

- Alcalá, S., Sancho, P., Martinelli, P., Navarro, D., Pedrero, C., Martín-Hijano, L., Valle, S., Earl, J., Rodríguez-Serrano, M., Ruiz-Cañas, L., et al. (2020). ISG15 and ISGylation is required for pancreatic cancer stem cell mitophagy and metabolic plasticity. *Nat. Commun.* *11*, 2682. <https://doi.org/10.1038/s41467-020-16395-2>.
- Angeletti, F., Fossati, G., Pattarozzi, A., Würth, R., Solari, A., Daga, A., Masiello, I., Barbieri, F., Florio, T., and Comincini, S. (2016). Inhibition of the autophagy pathway synergistically potentiates the cytotoxic activity of givinostat (ITF2357) on human glioblastoma cancer stem cells. *Front. Mol. Neurosci.* *9*, 107. <https://doi.org/10.1007/s10571-020-00891-6>.
- Carballo, G.B., and Ribeiro, J.H. (2020). GANT-61 Induces Autophagy and Apoptosis in Glioblastoma Cells Despite Their Heterogeneity. <https://doi.org/10.1007/s10571-020-00891-6>.
- Chan, D.C. (2020). Mitochondrial dynamics and its involvement in disease. *Annu. Rev. Pathol.* *15*, 235–259. <https://doi.org/10.1146/annurev-pathmechdis-012419-032711>.
- Das, M., Singh, S., Pradhan, S., and Narayan, G. (2014). MCM Paradox: Abundance of Eukaryotic Replicative Helicases and Genomic Integrity 2014, p. 574850. <https://doi.org/10.1155/2014/574850>.
- Dumit, V.I., Küttner, V., Käßler, J., Piera-Velazquez, S., Jimenez, S.A., Bruckner-Tuderman, L., Uitto, J., and Dengjel, J. (2014). Altered MCM protein levels and autophagic flux in aged and systemic sclerosis dermal fibroblasts. *J. Invest. Dermatol.* *134*, 2321–2330. <https://doi.org/10.1038/jid.2014.69>.
- García-Prat, L., Martínez-Vicente, M., Perdiguero, E., Ortet, L., Rodríguez-Ubrea, J., Rebollo, E., Ruiz-Bonilla, V., Gutarra, S., Ballestar, E., Serrano, A.L., et al. (2016). Autophagy maintains stemness by preventing senescence. *Nature* *529*, 37–42. <https://doi.org/10.1038/nature16187>.
- Guan, Y.B., Yang, D.R., Nong, S.J., Ni, J., Hu, C.H., Li, J., Zhu, J., and Shan, Y.X. (2017). Brevescapine (BVP) inhibits prostate cancer progression through damaging DNA by minichromosome maintenance protein-7 (MCM-7) modulation. *Biomed. Pharmacother.* *93*, 103–116. <https://doi.org/10.1016/j.biopha.2017.06.024>.
- Han, S., Jeong, Y.Y., Sheshadri, P., Su, X., and Cai, Q. (2020). Mitophagy regulates integrity of mitochondria at synapses and is critical for synaptic maintenance. *EMBO Rep.* *21*, e49801. <https://doi.org/10.15252/embr.201949801>.
- Han, Y., Fan, S., Qin, T., Yang, J., Sun, Y., Lu, Y., Mao, J., and Li, L. (2018). Role of autophagy in breast cancer and breast cancer stem cells (Review). *Int. J. Oncol.* *52*, 1057–1070. <https://doi.org/10.3892/ijo.2018.4270>.
- Herzig, S., and Shaw, R.J. (2018). AMPK: guardian of metabolism and mitochondrial homeostasis. *Nat. Rev. Mol. Cell Biol.* *19*, 121–135. <https://doi.org/10.1038/nrm.2017.95>.
- James, N.D., Hussain, S.A., Hall, E., Jenkins, P., Tremlett, J., Rawlings, C., Crundwell, M., Sizer, B., Sreenivasan, T., Hendron, C., et al. (2012). Radiotherapy with or without chemotherapy in muscle-invasive bladder cancer. *N. Engl. J. Med.* *366*, 1477–1488. <https://doi.org/10.1056/NEJMoa1106106>.
- Jia, M., Su, B., Mo, L., Qiu, W., Ying, J., Lin, P., Yang, B., Li, D., Wang, D., Xu, L., et al. (2021). Circadian clock protein CRY1 prevents paclitaxel-induced senescence of bladder cancer cells by promoting p53 degradation. *Oncol. Rep.* *45*, 1033–1043. <https://doi.org/10.3892/or.2020.7914>.
- Kim, J., Kundu, M., Viollet, B., and Guan, K.L. (2011). AMPK and mTOR regulate autophagy through direct phosphorylation of Ulk1. *Nat. Cell Biol.* *13*, 132–141. <https://doi.org/10.1038/ncb2152>.
- Kim, S., Cho, H., Hong, S.O., Oh, S.J., Lee, H.J., Cho, E., Woo, S.R., Song, J.S., Chung, J.Y., and Son, S.W. (2020). LC3B Upregulation by NANOG Promotes Immune Resistance and Stem-like Property through Hyperactivation of EGFR Signaling in Immune-Refractory Tumor Cells, pp. 1–20. <https://doi.org/10.1080/15548627.2020.1805214>.
- Kimura, S., Noda, T., and Yoshimori, T. (2007). Dissection of the autophagosome maturation process by a novel reporter protein, tandem fluorescently-tagged LC3. *Autophagy* *3*, 452–460. <https://doi.org/10.4161/auto.4451>.
- Kimura, S., Noda, T., and Yoshimori, T. (2008). Dynein-dependent movement of autophagosomes mediates efficient encounters with lysosomes. *Cell Struct. Funct.* *33*, 109–122. <https://doi.org/10.1247/csf.08005>.
- Kong, L., Yin, H., and Yuan, L. (2017). Centrosomal MCM7 strengthens the Cep68-VHL interaction and excessive MCM7 leads to centrosome splitting resulting from increase in Cep68 ubiquitination and proteasomal degradation. *Biochem. Biophys. Res. Commun.* *489*, 497–502. <https://doi.org/10.1016/j.bbrc.2017.05.180>.
- Kudo, Y., Sugimoto, M., Arias, E., Kasashima, H., Cordes, T., Linares, J.F., Duran, A., Nakanishi, Y., Nakanishi, N., L'Hermitte, A., et al. (2020). Pkc λ loss induces autophagy, oxidative phosphorylation, and NRF2 to promote liver cancer progression. *Cancer Cell* *38*, 247–262.e11. <https://doi.org/10.1016/j.ccell.2020.05.018>.
- Lamia, K.A., Sachdeva, U.M., DiTacchio, L., Williams, E.C., Alvarez, J.G., Egan, D.F., Vasquez, D.S., Juguilon, H., Panda, S., Shaw, R.J., et al. (2009). AMPK regulates the circadian clock by cryptochrome phosphorylation and degradation. *Science* *326*, 437–440. <https://doi.org/10.1126/science.1172156>.
- Li, J., Chen, X., Kang, R., Zeh, H., and Klionsky, D.J. (2020). Regulation and Function of Autophagy in Pancreatic Cancer, pp. 1–22. <https://doi.org/10.1080/15548627.2020.1847462>.
- Li, Y., and Chen, Y. (2019). AMPK and autophagy. *Adv. Exp. Med. Biol.* *1206*, 85–108. https://doi.org/10.1007/978-981-15-0602-4_4.
- Li, Z., and Xu, X. (2019). Post-translational modifications of the mini-chromosome maintenance proteins in DNA replication. *Genes* *10*, E331. <https://doi.org/10.3390/genes10050331>.
- Liang, Z., Li, W., Liu, J., Li, J., He, F., Jiang, Y., Yang, L., Li, P., Wang, B., Wang, Y., et al. (2017). Simvastatin suppresses the DNA replication licensing factor MCM7 and inhibits the growth of tamoxifen-resistant breast cancer cells. *Sci. Rep.* *7*, 41776. <https://doi.org/10.1038/srep41776>.
- Liu, K., Lee, J., Kim, J.Y., Wang, L., Tian, Y., Chan, S.T., Cho, C., Machida, K., Chen, D., and Ou, J.H.J. (2017). Mitophagy controls the activities of tumor suppressor p53 to regulate hepatic cancer stem cells. *Mol. Cell* *68*, 281–292.e5. <https://doi.org/10.1016/j.molcel.2017.09.022>.
- Mackeh, R., Perdiz, D., Lorin, S., Codogno, P., and Poüs, C. (2013). Autophagy and microtubules – new story, old players. *J. Cell Sci.* *126*, 1071–1080. <https://doi.org/10.1242/jcs.115626>.
- Maejima, Y., Kyoji, S., Zhai, P., Liu, T., Li, H., Ivessa, A., Sciarretta, S., Del Re, D.P., Zablocki, D.K., Hsu, C.P., et al. (2013). Mst1 inhibits autophagy by promoting the interaction between Beclin1 and Bcl-2. *Nat. Med.* *19*, 1478–1488. <https://doi.org/10.1038/nm.3322>.
- Najafi, M., Mortezaee, K., and Majidpoor, J. (2019). Cancer stem cell (CSC) resistance drivers. *Life Sci.* *234*, 116781. <https://doi.org/10.1016/j.lfs.2019.116781>.
- Nazio, F., Bordi, M., Cianfanelli, V., Locatelli, F., and Cecconi, F. (2019). Autophagy and cancer stem cells: molecular mechanisms and therapeutic applications. *Cell Death Differ.* *26*, 690–702. <https://doi.org/10.1038/s41418-019-0292-y>.
- Olejniczak-Kęder, A., Szaryńska, M., Wrońska, A., Siedlecka-Kroplewska, K., and Kmiec, Z. (2019). Effects of 5-FU and anti-EGFR antibody in combination with ASA on the spherical culture system of HCT116 and HT29 colorectal cancer cell lines. *Int. J. Oncol.* *55*, 223–242. <https://doi.org/10.3892/ijo.2019.4809>.
- Parikh, R.B., Adamson, B.J.S., Khozin, S., Galsky, M.D., Baxi, S.S., Cohen, A., and Mamtani, R. (2019). Association between FDA label restriction and immunotherapy and chemotherapy use in bladder cancer. *JAMA* *322*, 1209–1211. <https://doi.org/10.1001/jama.2019.10650>.
- Parlanti, E., Locatelli, G., Maga, G., and Dogliotti, E. (2007). Human base excision repair complex is physically associated to DNA replication and cell cycle regulatory proteins. *Nucleic Acids Res.* *35*, 1569–1577. <https://doi.org/10.1093/nar/gkl1159>.
- Pattingre, S., Tassa, A., Qu, X., Garuti, R., Liang, X.H., Mizushima, N., Packer, M., Schneider, M.D., and Levine, B. (2005). Bcl-2 antiapoptotic proteins inhibit Beclin 1-dependent autophagy. *Cell* *122*, 927–939. <https://doi.org/10.1016/j.cell.2005.07.002>.
- Praharaj, P.P., Panigrahi, D.P., Bhol, C.S., Patra, S., Mishra, S.R., Mahapatra, K.K., Behera, B.P., Singh, A., Patil, S., and Bhutia, S.K. (2021). Mitochondrial rewiring through mitophagy and mitochondrial biogenesis in cancer stem cells: a potential target for anti-CSC cancer therapy. *Cancer Lett.* *498*, 217–228. <https://doi.org/10.1016/j.canlet.2020.10.036>.
- Qu, K., Wang, Z., Fan, H., Li, J., Liu, J., Li, P., Liang, Z., An, H., Jiang, Y., Lin, Q., et al. (2017). MCM7

promotes cancer progression through cyclin D1-dependent signaling and serves as a prognostic marker for patients with hepatocellular carcinoma. *Cell Death Dis.* **8**, e2603. <https://doi.org/10.1038/cddis.2016.352>.

Qureshi-Baig, K., Kuhn, D., Viry, E., Pozdeev, V.I., Schmitz, M., Rodriguez, F., Ullmann, P., Koncina, E., Nurmik, M., Frاسquilho, S., et al. (2020). Hypoxia-induced autophagy drives colorectal cancer initiation and progression by activating the PRKC/PKC-EZR (ezrin) pathway. *Autophagy* **16**, 1436–1452. <https://doi.org/10.1080/15548627.2019.1687213>.

Ren, B., Yu, G., Tseng, G.C., Cieply, K., Gavel, T., Nelson, J., Michalopoulos, G., Yu, Y.P., and Luo, J.H. (2006). MCM7 amplification and overexpression are associated with prostate cancer progression. *Oncogene* **25**, 1090–1098. <https://doi.org/10.1038/sj.onc.1209134>.

Sancho, P., Barneda, D., and Heeschen, C. (2016). Hallmarks of cancer stem cell metabolism. *Br. J. Cancer* **114**, 1305–1312. <https://doi.org/10.1038/bjc.2016.152>.

Siegel, R.L., Miller, K.D., Fuchs, H.E., and Jemal, A. (2021). *Cancer Statistics, 2021*. CA. *Cancer J.*

Clin. **71**, 7–33. <https://doi.org/10.3322/caac.21654>.

Smith, A.G., and Macleod, K.F. (2019). Autophagy, cancer stem cells and drug resistance. *J. Pathol.* **247**, 708–718. <https://doi.org/10.1002/path.5222>.

Takahashi, J.S. (2017). Transcriptional architecture of the mammalian circadian clock. *Nat. Rev. Genet.* **18**, 164–179. <https://doi.org/10.1038/nrg.2016.150>.

Wang, H.Y., Zhang, B., Zhou, J.N., Wang, D.X., Xu, Y.C., Zeng, Q., Jia, Y.L., Xi, J.F., Nan, X., He, L.J., et al. (2019). Arsenic trioxide inhibits liver cancer stem cells and metastasis by targeting SRF/MCM7 complex. *Cell Death Dis.* **10**, 453. <https://doi.org/10.1038/s41419-019-1676-0>.

Whelan, K.A., Chandramouleeswaran, P.M., Tanaka, K., Natsuzaka, M., Guha, M., Srinivasan, S., Darling, D.S., Kita, Y., Natsugoe, S., Winkler, J.D., et al. (2017). Autophagy supports generation of cells with high CD44 expression via modulation of oxidative stress and Parkin-mediated mitochondrial clearance. *Oncogene* **36**, 4843–4858. <https://doi.org/10.1038/ncr.2017.102>.

Yamamoto, K., Venida, A., Yano, J., Biancur, D.E., Kakiuchi, M., Gupta, S., Sohn, A.S.W., Mukhopadhyay, S., Lin, E.Y., Parker, S.J., et al. (2020). Autophagy promotes immune evasion of pancreatic cancer by degrading MHC-I. *Nature* **581**, 100–105. <https://doi.org/10.1038/s41586-020-2229-5>.

Zhang, D., Wang, W., Sun, X., Xu, D., Wang, C., Zhang, Q., Wang, H., Luo, W., Chen, Y., Chen, H., and Liu, Z. (2016). AMPK regulates autophagy by phosphorylating BECN1 at threonine 388. *Autophagy* **12**, 1447–1459. <https://doi.org/10.1080/15548627.2016.1185576>.

Srivastava, A.K., Banerjee, A., Cui, T., Han, C., Cai, S., Liu, L., Wu, D., Cui, R., Li, Z., Zhang, X., et al. (2019). Cancer stem cells (CSCs) in cancer progression and therapy. *Cancer Res.* **79**, 2314–2326. <https://doi.org/10.1002/jcp.27740>.

Zheng, D., Ye, S., Wang, X., Zhang, Y., Yan, D., Cai, X., Gao, W., Shan, H., Gao, Y., Chen, J., et al. (2017). Pre-RC Protein MCM7 depletion promotes mitotic exit by inhibiting CDK1 activity. *Sci. Rep.* **7**, 2854. <https://doi.org/10.1038/s41598-017-03148-3>.

STAR★METHODS

KEY RESOURCES TABLE

REAGENT or RESOURCE	SOURCE	IDENTIFIER
Antibodies		
Anti-LC3B	Abcam	Cat # ab239416; RRID:AB_2923298
Anti-SQSTM1/p62	Abcam	Cat # ab280086; RRID:AB_2923299
Anti-ATP5A	Abcam	Cat# ab14748; RRID:AB_301447
Anti-rabbit IgG (H+L)	Cell Signaling	Cat# 4414; RRID:AB_10693544
Anti-mouse IgG (H+L)	Cell Signaling	Cat# 4408; RRID:AB_10694704
Anti-MCM7	Abcam	Cat# ab52489;RRID:AB_881187
Anti- Sox2	Cell Signaling	Cat# 14962; RRID:AB_2798664
Anti-GAPDH antibody	Abcam	Cat# ab9485; RRID:AB_307275
Anti-MCM2	Cell Signaling	Cat# 4007; RRID:AB_2142134
Anti-MCM3	Cell Signaling	Cat# 4012; RRID:AB_2235150
Anti-Cyclin B1	Abcam	Cat# ab32053; RRID:AB_731779
Anti-Cyclin D1	Abcam	Cat# ab16663; RRID:AB_443423
Anti-Nanog	Cell Signaling	Cat# 4903; RRID:AB_10559205
Anti-Sox2	Cell Signaling	Cat# 14962; RRID:AB_2798664
Anti-Oct4	Cell Signaling	Cat# 2750, RRID:AB_823583
Anti-SQSTM1/p62	Abcam	Cat# ab109012; RRID:AB_2810880
Anti-LC3B	Abcam	Cat# ab192890; RRID:AB_2827794
Anti-Beclin-1	Cell Signaling	Cat# 3495, RRID:AB_1903911
Anti-BNIP3	Abcam	Cat# ab10433; RRID:AB_2066656
Anti-PINK1	Abcam	Cat# ab23707; RRID:AB_447627
Anti-AMPK alpha 1	Abcam	Cat# ab32047; RRID:AB_722764
Anti-AMPK alpha 1 (phospho T183)	Abcam	Cat # ab133448; RRID:AB_2923300
Anti-Bcl-2	Abcam	Cat# ab692; RRID:AB_305670
Anti-Bax	Abcam	Cat# ab32503; RRID:AB_725631
Anti-P53	Proteintech Group	Cat# 60283-2-Ig; RRID:AB_2881401
Anti-CRY1	Abcam	Cat# ab54649; RRID:AB_2276575
Anti-Cytoplasmic Dynein	Abcam	Cat# ab23905; RRID:AB_2096669
Goat Anti-Rabbit IgG H&L (HRP)	Abcam	Cat# ab7090; RRID:AB_955417
Goat Anti-Mouse IgG H&L (HRP)	Abcam	Cat# ab7068; RRID:AB_955413
Anti-CD133	eBioscience	Cat# 53-1338-42; RRID:AB_2815206
Anti-CD44	eBioscience	Cat# 12-0441-82; RRID:AB_465664
Anti-Bcl2	Cell Signaling	Cat# 15071, RRID:AB_2744528
Anti-GAPDH	Cell Signaling	Cat# 2118, RRID:AB_561053
Alexa Fluor 647anti-rabbit Ab	Cell Signaling	Cat# 4414, RRID:AB_10693544
Alexa Fluor 488 anti-mouse Ab	Cell Signaling	Cat# 4408; RRID:AB_10694704
Chemical, peptides, and recombinant proteins		
DMEM	Gibco	Cat. # 11965092
PBS	Gibco	Cat. # 10010072
Fetal bovine serum	Gibco	Cat. # 10099141C
DMEM/F12	Gibco	Cat. # A4192001

(Continued on next page)

Continued

REAGENT or RESOURCE	SOURCE	IDENTIFIER
Penicillin-Streptomycin	Gibco	Cat. # 15140148
Cisplatin	Sigma	Cat. #15663-27-1
Paclitaxel	Cell Signaling	Cat. # 9807S
EGF	Peprotech	Cat. # 27141-1-AP
FGF- β	Biovision	Cat. # 4036-10
LIF	MedChemExpress	Cat. # HY-P73276
B-27	Gibco	Cat. # 17504-044
BSA	Solarbio	N/A
Trizol	Invitrogen	Cat. # 10296010
protein A + G conjugated beads	Beyotime	Cat. #P2108
Lipofectamine 3000	Invitrogen	Cat. # lip3000

Critical commercial assays

Rabbit specific HRP/DAB (ABC) Detection IHC Kit	Abcam	Cat# ab64261
EdU detection kit	Ribobio	Cat# C10310003
Annexin V/FITC and PI apoptosis detection kit	eBioscience	Cat# BMS500FI-300
PrimeScript RT reagent Kit	TaKaRa	Cat# RR047A
ECL-kit	Fude Biology	Cat#FD8000
MTS assay kit	Abcam	Cat#ab197010
Seahorse XF Cell Mito Stress Test Kit	Agilent	Cat# 103015
Seahorse XF Glycolytic Rate Assay Kit	Agilent	Cat# 103344
BCA Protein Concentration Determination Kit	Beyotime	Cat# P0012S

Deposited data

Autophagy related genes	This paper	http://www.autophagy.lu/clustering/index.html
The clinical data of BC patients	This paper	TCGA-BLCA: https://portal.gdc.cancer.gov/

Experimental models: Cell lines

UMUC3 cell line	ATCC	Cat. # CRL-1749
EJ cell line	BNCC	Cat. # BNCC342285
Bladder cancer stem-like cells	This paper	N/A

Oligonucleotides

Primers, see Tables S1 and S2	This paper	N/A
---	------------	-----

Software and algorithms

SPSS 20.0	IBM	http://www.downxia.com
GraphPad Prism 5.0	GraphPad Software	http://www.ddooo.com/softdown/44298.htm
ImageJ	Schneider et al., 2012	https://imagej.nih.gov/ij/
FlowJo	Tree Star Inc.	http://www.treestar.com/
Image-ProPlus 6.0	N/A	https://www.jb51.net/softs/436046.html

RESOURCE AVAILABILITY

Lead contact

Further information and requests for resources and reagents should be directed to and will be fulfilled by the lead contact, Lijun Mo (molijun304@sina.com).

Materials availability

This study did not generate new unique reagents.

Data and code availability

- Autophagy related genes (ARG) were obtained from the human Autophagy database (HADb). The mRNA expression profiles and clinical dataset for BC patients were available through the Genomic Data Commons Data Portal (Project: TCGA-BLCA).
- This paper does not report original code.
- Any additional information required to reanalyze the data reported in this paper is available from the [lead contact](#) upon request.

EXPERIMENTAL MODEL AND SUBJECT DETAILS

BALB/c nude mice of both genders, aged 6–8 weeks were purchased from experimental animal center of Southern Medical University. All animal studies were done in accordance with the university guidelines for experimental animals and approved by the ethical committee of Southern Medical University, and the ethical code is SMUL2020134.

METHOD DETAILS

To obtain bladder cancer stem-like cells

UMUC3 and EJ were cultured in DMEM medium supplemented with 10% fetal bovine serum, penicillin (100 U/ml) and streptomycin (100 µg/ml), and then cultured at 37°C in humidified incubator with an atmosphere of 5% CO₂. Cisplatin-resistant UMUC-3 and EJ cells were obtained by continuously treatment with 4 µg/ml Cisplatin changing fresh medium every 2 days for 30 days. The resistant cells were then kept in 2 µg/ml Cisplatin. BCSLCs were obtained by culturing the resistant cells in the medium with 4 µg/ml Cisplatin for 5 days.

Cell viability measurement

UMUC3, EJ cells and their according Cisplatin-resistant cells (UMUC3R or EJ_R) were inoculated into 96-well plates and then incubated with different concentrations of Cisplatin (0–40 µg/ml) or Paclitaxel (0–1000 nM) for 24 h. Cell viability was determined by microplate reader using MTS assay kit. The results were expressed as mean ± SD viable cells relatively to drug vehicle alone (considered as 100% viability).

Spheroid formation

Resistant cells were cultured in the medium with 4 µg/ml Cisplatin for 5 days, and then were laid on a low adhesion culture plate and cultured in serum-free DMEM/F12 medium (EGF 20 ng/ml, bFGF 20 ng/ml, LIF 20 ng/ml, B27 20 µl/ml and BSA 4 µg/ml) for 3 days. Spheroid formation was observed under microscope.

Quantitative real-time PCR

Total RNA was isolated from cells (UMUC3, UMUC3R, EJ and EJ_R) using Trizol® reagent, and reversed transcribed using a PrimeScript RT reagent Kit with gDNA Eraser. Real-time PCR was performed using the Applied Biosystems®7500 Real-Time PCR Systems. Then the reaction system is premixed according to the manufacturer's protocol with SYBR and cDNA. 95°C, 5 min are used to pre-denatured, 40 cycles for amplification (95°C, 10s, 60°C, 34s), then (95°C, 15s, 60°C, 1 min, 95°C, 15s) were used to obtain the dissolution curve. Real-time PCR quantification used 2- $\Delta\Delta$ Ct method against the *GAPDH* for normalization.

EdU incorporation assays

UMUC3, UMUC3-CSLCs, EJ and EJ CSLCs were planted in 24 well plates (1 × 10⁵ cells/well), and then DNA replication was detected by 5-ethynyl-2'-deoxyuridine (EdU) labeling/detection kit according to the manual instruction. EdU labeling medium (1:1000) was added into wells and incubated for 2 h as indicates and then cells were counterstained with Hoechst33342. The percentage of EdU⁺ cells was calculated from five random fields each in three wells.

Immuno-fluorescence

The cells were cultured on cell slide and were fixed with 4% paraformaldehyde for 30 min at room temperature, and then permeabilized by 0.2% Triton X-100 in phosphate-buffered saline for 10 min. The cell slides were incubated with primary antibodies against LC3B Rabbit mAb, Anti-SQSTM1/P62 Mouse mAb or anti-ATP5A Mouse mAb overnight at 4°C after blocking by 5% BSA for 1h. The cells were subsequently

incubated with Alexa Fluor 647 anti-rabbit Ab or Alexa Fluor 488 anti-mouse Ab according to the origin of the primary antibody species at 37°C for 1 h. The signals were detected by through confocal microscope.

Immunohistochemistry

Subcutaneous tumor tissues were collected from each experiment group on days 30 after BCSLCs injection, and then embedded in paraffin after fixing with 4% paraformaldehyde. Paraffin sections (4–5 μm) were deparaffinized and rehydrated and treated with hydrogen peroxide, followed by antigen retrieval. After blocking for 10 min, the sections were incubated with anti-MCM7 Rabbit mAb, Anti-Sox2 Rabbit mAb according to the manufacturer's instructions of Rabbit specific HRP/DAB (ABC) Detection IHC Kit and counterstained with hematoxylin.

Western blot

Total proteins of cells were extracted with ice-cold RIPA containing PMSF for 15 min. Equal amounts of protein were separated on 10% SDS-PAGE and then transferred to PVDF membranes. Subsequently, the membrane was blocked with 5% skim milk for 2 h at room temperature and incubated with primary antibodies in TBST overnight at 4°C. Primary antibodies against the following proteins were used: GAPDH, MCM7, MCM2, MCM3, Cyclin B, Cyclin D, NANOG, SOX2, OCT4, P62, LC3, BECLIN1, BNIP3, PINK1, AMPK, p-AMPK, BCL2, BAX and Dynein. The membranes were washed four times by TBST buffer and then incubated with Goat Anti-Rabbit IgG H&L (HRP) or Goat Anti-Mouse IgG H&L (HRP) according to the species of primary antibodies for 1 hour at room temperature. Protein binding was visualized using an Immobilon Western-HRP substrate.

Flow cytometry analysis

For apoptosis assay, cells were cultured in 6-well plates and interfered with MCM7 or treated with 20 μmol/L Metformin for 24 hours. The cell apoptosis was measured by flow cytometry using an annexin V/FITC and PI apoptosis detection kit according to the manufacturer. Briefly, 1×10^5 cells were resuspended in Annexin V binding buffer and then incubated with Annexin V-FITC and Propidium Iodide (1 μg/ml) for 15 min at room temperature and then detected by flow cytometry. For CD44⁺ and CD133⁺ analysis, cells were washed two times with PBS and stained with FITC Anti-CD133 antibody and PE Anti-CD44 antibody for 30 min and then measured by flow cytometer.

Co-immunoprecipitation (Co-IP)

The cells were lysed with RIPA lysis buffer containing 1 mM PMSF and phosphatase inhibitor after washing with cold PBS. Total cell lysates were incubated with 1 μg anti-BCL2 or anti-BECLIN1 or anti-Dynein overnight at 4°C, and then mixed with 40 μl protein A + G conjugated beads to each sample. Centrifuged at 4°C for 14,000 g for 15 min. Beads were then washed with lysis buffer and centrifugation was repeated three times. The immunoprecipitated protein complexes were analyzed via western blotting.

Analysis of autophagy related genes

Autophagy related genes (ARG) were obtained from the human Autophagy database (HADb). The mRNA expression profiles and clinical dataset for BC patients were extracted from the TCGA database (<https://cancergenome.nih.gov/>). A total of 414 BC samples and 19 normal samples were enrolled in this study to perform variance, GO enrichment and prognostic correlation analysis.

Seahorse XF96 metabolic flux analysis

Oxygen consumption rates and glycolytic rates were determined by Seahorse XF96, using the corresponding kits. 5,000 cells/well (in 80 μL) were seeded in the an XF 96-well cell culture microplate and then incubated overnight at 37°C in 5% CO₂. The Seahorse cartridge was submerged with sterile water overnight at 37°C in a non-CO₂ incubator and then humidified in prewarmed XF-calibrant solution for 45–60 min. On the next day, the cells were supplied with seahorse assay medium (XF RPMI medium, 1 mM pyruvate, 2 mM glutamine, 10 mM glucose, pH 7.4). For determination of oxidative respiration, 1 μM Oligomycin, 1 μM FCCP and 0.5 μM Rotenone/antimycin. All solutions were added to cartridge port A, B, or C. For determination of glycolytic rates, 0.5 μM Rotenone/Antimycin A and 50 mM 2-deoxy-glucose (2-DG) solutions were added to cartridge port A or B, respectively. Measurements were determined and shown by Test Report Generators (Agilent), and normalized to total cellular protein quantified by BCA Protein Concentration Determination Kit.

MCM7 silencing

In vitro MCM7 silencing was obtained by siRNA transfection with Lip3000, Si NC group was used as negative control. Cells were cultured with fresh DMEM medium 5 hours after transfection. Total RNA and protein of cells were extracted to verify the efficiency of MCM7 silencing after transfection 48 hours. *In vivo* MCM7 silencing was performed by lentivirus-mediated shRNA transfection. The recombinant lentivirus particles LV-MCM7 (labeled with red fluorescence and with ampicillin resistance) and control lentivirus particles LV-negative control (NC) were constructed.

Animal models

For the *in vivo* tumorigenicity assay of BCSCs, 1×10^5 BCSCs or bladder cancer cells were transplanted on the right leg root of nude BALB/c mice by subcutaneous injection (each group contained 6 mice). The mice were sacrificed after 4 weeks to observe tumor formation. For the *in vivo* MCM7 silencing assay, a total of 4×10^5 EJ-BCSCs were subcutaneously injected under the skin of the hind leg of BALB/c nude mice to establish subcutaneous tumor model. Mice were randomly divided into 2 groups on the 7th day after tumor cells inoculation, and were treated with 1×10^{11} TU viral vector LV-MCM7 or LV-NC (100 μ l/mouse) by intratumoral injection, once every 3 days, 5 times in total. The tumor growth was monitored every 4 days for 4 weeks. The tumor volume was calculated as follows: $V = [\pi/6(W1 \times W2 \times W2)]$.

QUANTIFICATION AND STATISTICAL ANALYSIS

Two-sided Student's t-tests, two-sided Chi-square test, Fisher's exact test, and multiple t-tests were performed using GraphPad Prism 5.0 and SPSS 20.0 software. Survival curves were analyzed and validated with the log-rank test. $P < 0.05$ were considered significant. Results are shown as means \pm S.D. The immunohistochemistry (IHC) staining intensity was analyzed using Image-ProPlus 6.0 software.